

Characterization of MIPS in a suspension of repulsive active Brownian particles through dynamical features

Cite as: J. Chem. Phys. **154**, 164901 (2021); <https://doi.org/10.1063/5.0040141>

Submitted: 10 December 2020 • Accepted: 02 April 2021 • Published Online: 22 April 2021

José Martin-Roca,  Raul Martinez, Lachlan C. Alexander, et al.



View Online



Export Citation



CrossMark

ARTICLES YOU MAY BE INTERESTED IN

Inertial effects of self-propelled particles: From active Brownian to active Langevin motion
The Journal of Chemical Physics **152**, 040901 (2020); <https://doi.org/10.1063/1.5134455>

The physics of active polymers and filaments
The Journal of Chemical Physics **153**, 040901 (2020); <https://doi.org/10.1063/5.0011466>

Inertial self-propelled particles
The Journal of Chemical Physics **154**, 024902 (2021); <https://doi.org/10.1063/5.0030940>

Lock-in Amplifiers
up to 600 MHz



Zurich
Instruments



Watch



Characterization of MIPS in a suspension of repulsive active Brownian particles through dynamical features

Cite as: J. Chem. Phys. 154, 164901 (2021); doi: 10.1063/5.0040141

Submitted: 10 December 2020 • Accepted: 2 April 2021 •

Published Online: 22 April 2021



José Martin-Roca,^{1,2} Raul Martinez,^{1,2,3}  Lachlan C. Alexander,⁴ Angel Luis Diez,^{1,2} Dirk G. A. L. Aarts,⁴ Francisco Alarcon,^{1,5} Jorge Ramirez,⁶  and Chantal Valeriani^{1,2,a)} 

AFFILIATIONS

¹Departamento de Estructura de la Materia, Física Térmica y Electrónica, Universidad Complutense de Madrid, 28040 Madrid, Spain

²GISC-Grupo Interdisciplinar de Sistemas Complejos, 28040 Madrid, Spain

³Departamento de Física Teórica de la Materia Condensada, Facultad de Ciencias, Universidad Autónoma de Madrid, 28049 Madrid, Spain

⁴Physical and Theoretical Chemistry Department, University of Oxford, Oxford, United Kingdom

⁵Departamento de Ingeniería Física, División de Ciencias e Ingenierías, Universidad de Guanajuato, Loma del Bosque 103, 37150 León, Mexico

⁶Departamento de Ingeniería Química, ETSI Industriales, Universidad Politécnica de Madrid, 28006 Madrid, Spain

^{a)} Author to whom correspondence should be addressed: cvaleriani@ucm.es

ABSTRACT

We study a two-dimensional system composed by Active Brownian Particles (ABPs), focusing on the onset of Motility Induced Phase Separation (MIPS), by means of molecular dynamics simulations. For a pure hard-disk system with no translational diffusion, the phase diagram would be completely determined by their density and Péclet number. In our model, two additional effects are present: translational noise and the overlap of particles; we study the effects of both in the phase space. As we show, the second effect can be mitigated if we use, instead of the standard Weeks–Chandler–Andersen potential, a stiffer potential: the pseudo-hard sphere potential. Moreover, in determining the boundary of our phase space, we explore different approaches to detect MIPS and conclude that observing dynamical features, via the non-Gaussian parameter, is more efficient than observing structural ones, such as through the local density distribution function. We also demonstrate that the Vogel–Fulcher equation successfully reproduces the decay of the diffusion as a function of density, with the exception of very high densities. Thus, in this regard, the ABP system behaves similar to a fragile glass.

Published under license by AIP Publishing. <https://doi.org/10.1063/5.0040141>

I. INTRODUCTION

Active matter is a branch of physics that studies out-of-equilibrium systems in which energy is supplied at the level of individual entities called active particles. Active particles dissipate energy while performing motion.^{1,2} Such out of equilibrium behavior can result in interesting collective phenomena not observed in equilibrium systems. Examples of collective motion of active living systems can be found at every length scale: from colonies of bacteria to flocks of birds.³ More recently, similar collective behavior has been

experimentally mimicked by synthetic active colloids,^{4–12} whose activity can be tuned either magnetically,^{13,14} chemically,^{15–17} via electric fields (thanks to induced-charge electrophoresis effects),^{18–20} or by means of UV light illumination.^{13,21,22}

On the theoretical side, models have been developed to get a better understanding of the physics of active matter, which might allow for the tailoring new smart materials. One of the simplest yet most insightful models is that of the so-called Active Brownian Particles (ABPs), where Brownian dynamics equations of motion have been modified to allow for particle self-propulsion and a

gradual change in the direction (tuned by rotational diffusion).^{23–26} One paradigmatic phenomenon observed in suspensions of repulsive ABPs is the emergence of Motility Induced Phase Separation (MIPS). Despite the lack of explicit attractive forces between particles, particles tend to phase separate into a dense region where they move slower and a dilute region where they move faster. MIPS, which can appear in either two^{27–31} or three dimensions,^{29,32} has been detected by computing the local density (a structural feature). Interesting questions have emerged from these studies, one of which is the role played by the active force on the particles' effective diameter, as briefly discussed in a previous work²⁹ where the Weeks–Chandler–Andersen (WCA) potential was used. The relative strength of the self-propulsion force and the repulsive inter-particle interaction force determines the distance between the particles in the denser regions of the simulation, as WCA allows some degree of overlap. Some studies, including studies of ABPs, have avoided overlap by using harder interaction potentials.^{25,33–35} The effect of the nature of the repulsive interaction on systems in thermodynamic equilibrium has been thoroughly studied.^{36–45} In this work, we provide a closer look on the effects determining the shape of the MIPS phase space and the importance of the softness of the potential.

The goal of our work is twofold: (i) to study the influence of different parameters (besides Péclet number and density) on the onset of MIPS and compare two potentials of different softness—the often used but relatively soft WCA⁴⁶ and a stiffer Pseudo-hard sphere potential (PHS),⁴⁷ a continuous potential that mimics structural and dynamical properties of hard-spheres in equilibrium^{47,48} and out-of-equilibrium.^{49,50} (ii) To study the system dynamics, we propose using dynamical properties, instead of structural ones, to locate the appearance of MIPS in the state diagram. In addition, we analyze the suitability of the Vogel–Fulcher equation for the description of the dynamical behavior of an ABP suspension as compared to its passive analog.

This manuscript is organized as follows: In Sec. II, we present the simulation details; in Sec. III, we show and discuss the results; and in Sec. IV, we present our conclusions.

II. SIMULATION DETAILS

The simulated system consists of $N = 20\,000$ circular particles with diameter σ in a two-dimensional box of size $L_x \times L_y$ (where periodic boundary conditions have been implemented). L_x and L_y have been set in order to obtain the desired total density $\rho = \frac{N}{L_x L_y}$ with a ratio $L_y/L_x \approx 0.58$. As in Ref. 51, we use the total density of the system instead of the packing fraction, since a particle diameter (needed to compute packing fraction) might not be uniquely defined due to particle activities (also cannot be estimated via Barker and Henderson's approach⁵²). As an initial configuration, we prepare the system in a hexagonal lattice. All simulations have been run at a given density until a steady-state is reached.

To simulate active Brownian particles, we perform Brownian dynamics simulations with an in house modified version of the LAMMPS⁵³ open source package. The equations of motion for the position \vec{r}_i and orientation θ_i of the i th active particle can be

written as

$$\dot{\vec{r}}_i = \frac{D_t}{k_B T} \left(- \sum_{j \neq i} \nabla V(r_{ij}) + F_a \vec{n}_i \right) + \sqrt{2D_t} \vec{\xi}_i, \quad (1)$$

$$\dot{\theta}_i = \sqrt{2D_r} \xi_{i,\theta}, \quad (2)$$

where $V(r_{ij})$ is the inter-particle pair potential, k_B is the Boltzmann constant, T is the absolute temperature, F_a is a constant self-propulsion force acting along the orientation vector \vec{n}_i , which forms an angle θ_i with the positive x -axis, D_t is the translational, and D_r is the rotational diffusion coefficient. Furthermore, the components of the thermal forces $\vec{\xi}_i$ and $\xi_{i,\theta}$ are white noise with zero mean and correlations $\langle \xi_i^\alpha(t) \xi_j^\beta(t') \rangle = \delta_{ij} \delta_{\alpha\beta} \delta(t - t')$, where α and β are the x and y components, respectively, and $\langle \xi_{i,\theta}(t) \xi_{j,\theta}(t') \rangle = \delta_{ij} \delta(t - t')$. In equilibrium, the translational, D_t , and rotational diffusion coefficient, D_r , follow a Stokes–Einstein relation for spherical particles (with diameter σ):⁵⁴ $D_r = 3D_t/\sigma^2$. However, when explicitly stated, we uncouple both diffusion coefficients. In an active matter system, this uncoupling is experimentally justified^{9–12} and has also been used in a previous work.²⁷ Although we have not found in the scientific literature a specific experimental system where D_r and D_t can be independently modified, we argue that there is no theoretical reason to affirm that this cannot be done in an active system, so this decoupling can also be of experimental interest.

Throughout our study, we will consider two repulsive interaction potentials (Fig. 1): WCA⁴⁶ potential (red),

$$V_{WCA}(r) = \begin{cases} 4\epsilon \left[\left(\frac{\sigma}{r} \right)^{12} - \left(\frac{\sigma}{r} \right)^6 \right] + \epsilon, & r < 2^{1/6} \sigma \\ 0, & r \geq 2^{1/6} \sigma, \end{cases} \quad (3)$$

where r is the center-to-center distance and σ is the particle diameter, and the so-called pseudo-hard sphere (PHS)⁴⁷ potential (blue),

$$V_{PHS}(r) = \begin{cases} 50 \left(\frac{50}{49} \right)^{49} \epsilon \left[\left(\frac{\sigma}{r} \right)^{50} - \left(\frac{\sigma}{r} \right)^{49} \right] + \epsilon, & r < \left(\frac{50}{49} \right) \sigma \\ 0, & r \geq \left(\frac{50}{49} \right) \sigma, \end{cases} \quad (4)$$

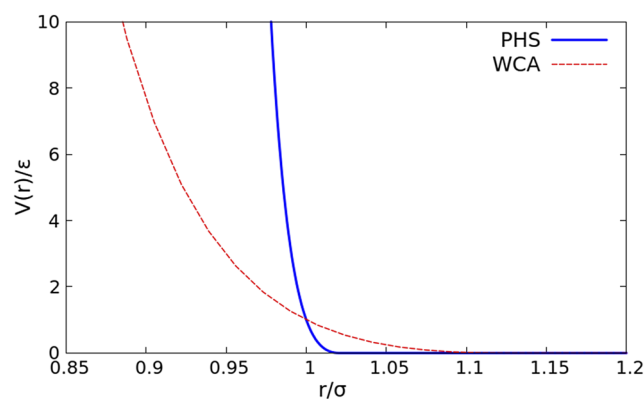


FIG. 1. Repulsive potentials considered in this work. Note that WCA is softer than PHS.

which has been shown to properly reproduce equilibrium⁴⁸ and out-of-equilibrium^{49,50} features of a hard sphere suspension.

Throughout this paper, all quantities are expressed in reduced units in which lengths, times, and energies are given in terms of σ , $\tau_{LJ} = \sqrt{m\sigma/\epsilon}$, and ϵ , respectively. In all our simulations, we set $\epsilon = 1$ and $D_t\tau_{LJ}/\sigma^2 = 1.5$ (value that will be clarified below), and the relation $D_t\tau_{LJ}/\sigma^2 = k_B T/\epsilon$. The time step is set to $\Delta t = 10^{-5}\tau_{LJ}$ for WCA and $\Delta t = 10^{-6}\tau_{LJ}$ for PHS.²⁹ We run the simulations for 10^7 steps for WCA and 10^8 steps for PHS to equilibrate the system. Then, we simulate another 10^8 steps for WCA and 10^9 steps for PHS. All our simulations are run for $t/\tau_{LJ} = 10^3$.

As a measure of the degree of activity, we use the Péclet number Pe , i.e., the dimensionless ratio between advective and diffusive transport, defined as

$$Pe = \frac{3v\tau_r}{\sigma} = \frac{3F_a D_t}{\sigma k_B T D_r}, \quad (5)$$

where $v = F_a D_t/k_B T$ is the self-propelling velocity and $\tau_r = 1/D_r$ is the reorientation time.

First, in order to detect phase separation, we follow Ref. 29 and compute the local density ρ_0 for each particle as the inverse of the area of the polygon associated with it via a Voronoi tessellation. The overall density ρ is the mean of ρ_0 averaged over all particles. To establish if the system phase separates into a dense and a dilute phase (MIPS), we calculate the probability distribution function (PDF) of the local density $P(\rho_0)$ (once the system is in the stationary state). Typically, when the system is homogeneous, $P(\rho_0)$ is characterized by a single maximum around the system average density. When MIPS occurs, $P(\rho_0)$ exhibits two maxima: one centered at the value of the local density characterizing the dilute phase and the other one corresponding to the concentrated phase. While the two $P(\rho_0)$ peaks are well defined deep into the MIPS region, they are not easily distinguishable near the boundary of the MIPS region.

For a better understanding of the local structure of dense phases, we compute the hexatic order parameter ψ_6 for the k th particle in two dimensions as

$$\psi_6(k) = \frac{1}{n} \sum_{j \in N_k} e^{i6\theta_{kj}}, \quad (6)$$

where θ_{kj} is the angle between the vector \vec{r}_{kj} and the x-axis, N_k is the set of first Voronoi neighbors⁵⁵ of particle k , and n is the number of neighbors. To compute the global crystalline order, we sum the value of $\psi_6(k)$ over all particles in the system.

As an alternative method to identify MIPS, besides computing the local density $P(\rho_0)$, we propose a method based on dynamical, rather than structural, properties. When MIPS starts, the system is characterized by dense regions of slow particles and dilute regions of fast particles, resembling dynamic heterogeneities observed in supercooled liquids.⁵⁶ Therefore, we investigate the dynamical heterogeneity appearing in the system by means of the non-Gaussian parameter, which in a two-dimensional system is

$$\alpha_2(t) = \frac{\langle \Delta r^4(t) \rangle}{2(\langle \Delta r^2(t) \rangle)^2} - 1, \quad (7)$$

where $\langle \Delta r^k(t) \rangle$ is the k th moment of the probability distribution function (PDF) of particle displacements in two dimensions. This

parameter is a measure of the deviation between the PDF and a Gaussian distribution, characteristic of pure Brownian motion. The non-Gaussian parameter has been previously used to describe anomalous and/or heterogeneous transport dynamics in systems at equilibrium or approaching the glassy state.^{57–61} In this work, for each simulation, we define σ_α as the characteristic size of the fluctuations of α_2 at equilibrium for the passive case at the same density. Thus, the proposed criterion to identify MIPS is as follows: (1) we compute the time evolution of α_2 ; (2) when this average is smaller than $10 \cdot \sigma_\alpha$, the system is in a homogeneous phase; and (3) when this average is larger than $10 \cdot \sigma_\alpha$, the system is in a MIPS state. The suitability of this method is discussed in Sec. III B. For further details on the meaning of the parameter σ_α and how to estimate its value for each system, see the [supplementary material](#).

To better unravel the dynamical features of the system, we also compute the long time effective diffusion coefficient D_{eff} from the slope of the mean-square displacement at long times. Inspired by the dynamical features of a metastable fluid, we try to fit the D_{eff} with the Vogel–Fulcher model (as in Ref. 62),

$$D_{\text{eff}}(\rho) = \exp\left(A + \frac{B}{\rho - \rho'}\right), \quad (8)$$

an empirical law frequently used in the study of glassy dynamics.⁶³

III. RESULTS

A. Density vs activity state diagrams

The phase space of an ABP suspension is typically characterized by two variables: the total density ρ and the Péclet number, Pe . However, according to Eq. (5), Pe can be varied by changing the temperature T (as in Ref. 29), the self-propelling force F_a (closely resembling experiments¹⁰), or the rotational diffusion coefficient D_r (as in Ref. 64). In this work, we attempt to quantify how the system phase behavior changes when different approaches are used to modify Pe .

In Fig. 2, we present three state diagrams for both WCA (left-hand side) and PHS (right-hand side) potentials, obtained by (a) changing $k_B T$ (while keeping $\epsilon = 1$ and all other parameters fixed); (b) changing D_r (while leaving all other parameters fixed, including D_t , thus not coupling the diffusion coefficients via the Stokes–Einstein relationship); and (c) changing F_a (while keeping all other parameters fixed). A figure where all diagrams are overlaid can be found in the [supplementary material](#). In each panel, the system undergoes motility induced phase separation (MIPS, solid symbols) when both density and activity (Péclet number) increase, and it can be found in an homogeneous phase at low density/activity (empty symbols). The same results have been obtained characterizing the different states via the local density (symbols) or non-Gaussian parameter α_2 (red dashed lines, discussed in Sec. III. B). By visual inspection, we can already state that the different parameters chosen to vary the Péclet mostly affect the boundaries of the MIPS phase, rather than its bulk.^{65,80}

In Figs. 2(a)–2(c), the Péclet is varied by changing $k_B T$, D_r , and F_a , respectively. The three diagrams coincide when $Pe = 16$ is the value of all the coefficients, which defines that Pe are the same. A detailed discussion on a way to compare the different diagrams can be found in the [supplementary material](#). Taking this into account,

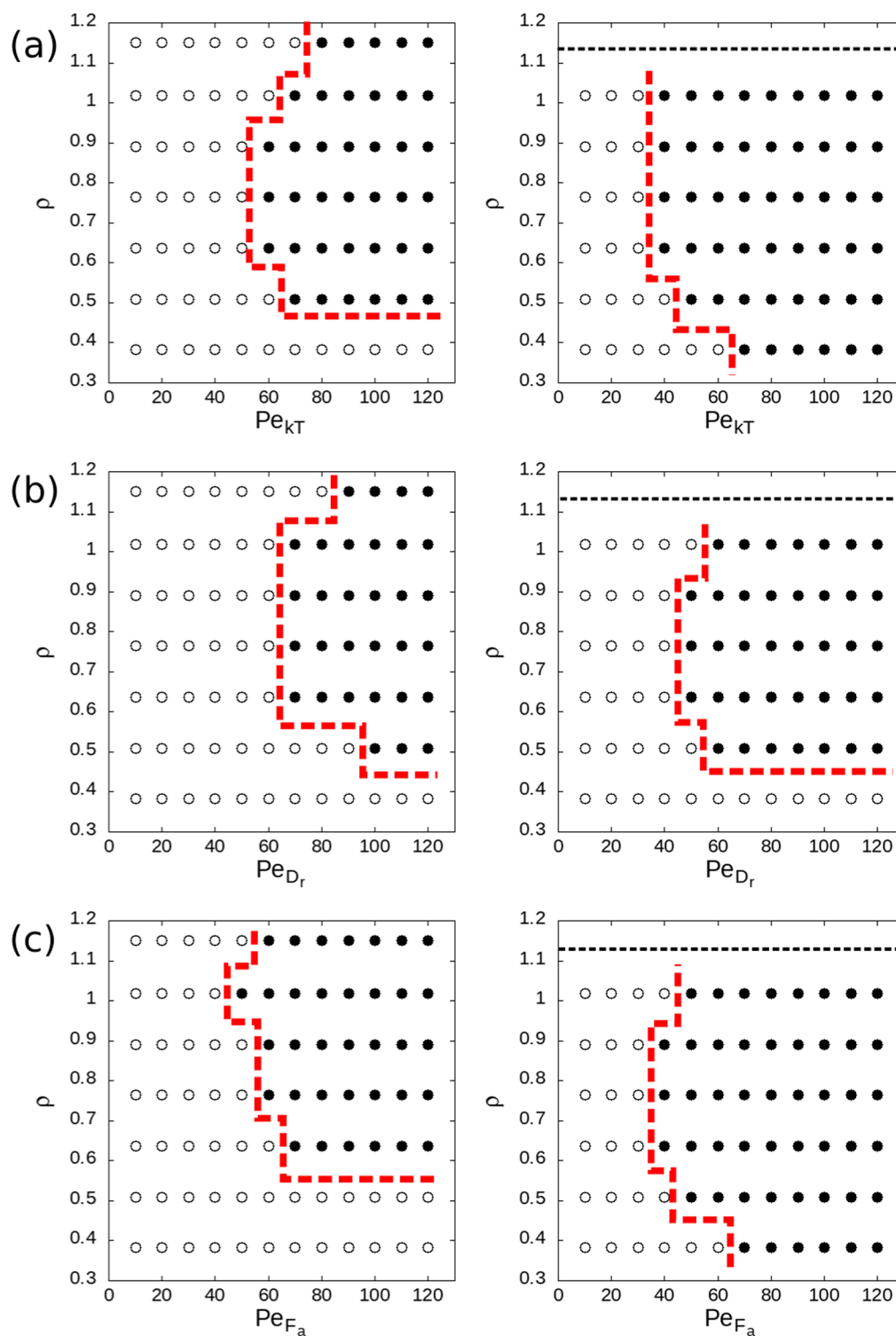


FIG. 2. p vs Pe state diagrams of ABP interacting by means of WCA (left) and PHS (right) potentials. Pe is modified by varying (a) $k_B T$ while keeping $D_r = 4.5$, $D_t = 1.5$, and $F_a \sigma / \varepsilon = 24$; (b) by varying D_r while keeping $k_B T / \varepsilon = 1.5$, $D_t = 1.5$, and $F_a \sigma / \varepsilon = 24$ fixed; and (c) by varying F_a while keeping $k_B T / \varepsilon = 1.5$ with $D_t = 1.5$ and D_r coupled. Black solid circles correspond to MIPS, and empty circles correspond to the homogeneous phase determined by $P(\rho_0)$.²⁹ Red dashed lines represent MIPS boundaries determined by means of the non-Gaussian parameter α_2 (see the main text).

from the comparison between (1) the state diagrams in Figs. 2(a) and 2(b) and (2) the phase diagrams in Figs. 2(a) and 2(c), we can isolate the influence of the following two physical properties:

1. Translational diffusion in the case where D_r is reduced to increase Pe [Fig. 2(b)] is less than when $k_B T$ is reduced [Fig. 2(a)] for a given Pe (leaving all else unchanged). The phase diagrams for both WCA and PHS in Fig. 2(b) show a shift of the MIPS boundary toward higher ρ and Pe when compared to Fig. 2(a). This preference for the homogeneous state suggests that a greater effective translational diffusion hinders MIPS.
2. When increasing F_a , the relative strength of the force leading to collisions compared to the repulsive force increases. This is not the case when $k_B T$ is reduced. Therefore, for a given Péclet number, the particles are effectively softer when F_a is increased. This is visible when Fig. 2(c) is compared to Fig. 2(a). When using the WCA potential, the softer potential, changing F_a shifts the MIPS boundary to higher Péclet numbers and densities. However, there are fewer differences when using the harder PHS potential. This indicates that the WCA potential is not a good representation for hard disks in the range of parameters used in this work. The PHS potential seems to be strong enough to prevent any significant particle overlap in both methods. Note that the previous version is very unclear.

To study the structural features of the ABP suspensions, we compute the value of ψ_6 for each particle [Eq. (6), to get information on the local crystalline order] and on the entire system (averaging over all particles, to get information on the global crystalline order).

In Figs. 3(a) and 3(b), we show different snapshots for the PHS and WCA systems, respectively (see the [supplementary material](#) for a bigger version of these panels). The color code reflects the value of ψ_6 for each particle, ranging from low (green) to high (red) local crystalline order. Independent of the interaction potential, we identify three main outcomes: (1) a homogeneous dilute phase of disordered particles (mostly green particles); (2) a MIPS phase, characterized by a dense phase (red particles) and a dilute phase (green particles); and (3) a homogeneous dense phase of mostly ordered particles (red). Interestingly, for the WCA-ABP suspension, MIPS is shifted toward higher densities due to a lower effective diameter arising from partial particle overlap.⁵¹

Clearly, the stiffness of the interaction potential not only has a considerable effect on the shape of the phase diagram (as shown in Fig. 2) but also affects how particles are ordered inside the dense phase. In Fig. 3(c) (WCA) and Fig. 3(d) (PHS), we show how the global order parameter changes when varying ρ and Pe_{Dr} . At low densities, both systems are disordered, independent of the value of the activity Pe_{Dr} . However, when increasing the density, $\langle\psi_6\rangle$ starts increasing for values of Pe_{Dr} in close correspondence to the appearance of MIPS.

When comparing the two interaction potentials, WCA particles have a lower hexatic order than PHS ones at the same densities and Pe_{Dr} values. This is because WCA particles partially overlap, whereas hard disks must organize with a higher hexagonal order at high density.

It is interesting to note that ψ_6 is not a good indicator to locate the MIPS boundaries at least for high density systems because its value strongly depends on the density, making it difficult to define a unique threshold value of ψ_6 that can help detect MIPS. Moreover, as shown in Figs. 3(c) and 3(d), the difference in $\langle\psi_6\rangle$ between MIPS and homogeneous states is not so clear at high densities. Some of the selected snapshots (corresponding to high densities and low Pe number, especially for the PHS potential) are characterized by a relatively large average value of ψ_6 . However, these are regions of the state diagram where no MIPS has been detected by neither the local density nor the non-Gaussian parameter (see Fig. 2).

B. Using the non-Gaussian parameter as a way to identify MIPS

In Sec. III A, we study the phase behavior of soft-like (WCA) and hard-like (PHS) excluded-volume potentials, determining MIPS regions (via the local density). We explore how different ways of modifying the Péclet number can affect the shape and location of the MIPS boundary in the state diagram, depending on the stiffness of the interaction potential. MIPS, characterized by the appearance of high/low density regions, is identified via static properties such as the probability distribution function of the local density $P(\rho_0)$ and structurally characterized by ψ_6 . Although the static and spatial inhomogeneities are frequently used to identify MIPS, it is clear that MIPS states are also characterized by a very large dynamical heterogeneity: in high density regions, particles are almost stagnant,

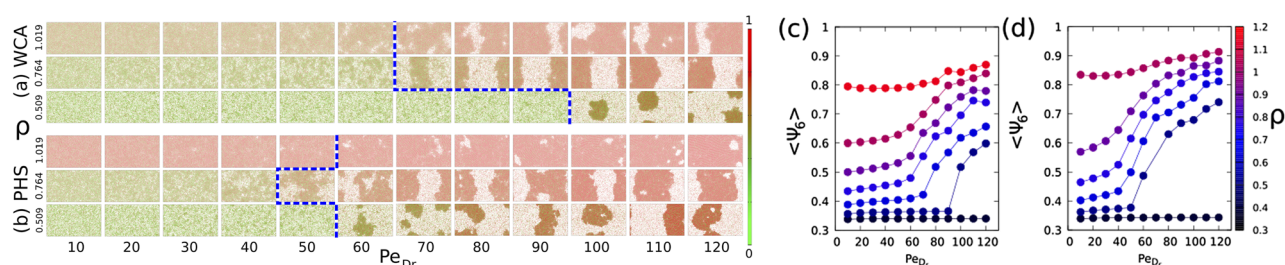


FIG. 3. (a) WCA and (b) PHS snapshots of the system in steady-state at selected points of the ρ - Pe_{Dr} state diagram (as indicated in the vertical/bottom axes). The color code corresponds to the local ψ_6 order, ranging from 0 (low order, green) to 1 (high order, red), and the blue dashed line corresponds to the boundary of MIPS in Fig. 2(b). (c) WCA and (d) PHS represent the global value of ψ_6 (averaged over all particles in the system) for all points in the ρ - Pe_{Dr} state diagram. Empty and filled dots represent homogeneous and MIPS states, respectively, with the same criteria used in Fig. 2 [see panel (b)].

whereas in low density regions, some particles may move very fast during the short periods of time between collisions.

The same behavior is characteristic of metastable fluids, where dynamic heterogeneities are present. When studying colloidal suspensions, Weeks *et al.*⁶⁰ demonstrated that for purely diffusive particles, the distribution of particles displacements was Gaussian. However, deviations from a Gaussian start to appear when the system becomes metastable (e.g., over-compressed) and can be quantified by a non-Gaussian parameter α_2 (which is exactly zero for a Gaussian distribution⁶⁶). When approaching the glass transition packing fraction, the value of α_2 increases. This is a sign of the fact that the system is characterized by spatially correlated aggregates of fast particles in a “sea” of slow particles.^{67–70}

Thus, when a fluid-like system is in a homogeneous state, the particle displacement is expected to be Gaussian, even in the presence of activity. Between collisions, the equation of motion has two terms: the diffusive term (which always yields Gaussian distributions) and the self-propulsion term. The random nature of particle collisions creates trajectories that are very similar to random flights after just a few collision events. Therefore, we expect that particle displacement should be Gaussian in homogeneous states, at least for times longer than the average times between collisions. However, when MIPS occurs, the system separates in phases of very different mobility, which strongly affects the Gaussianity of the displacements distribution. This has inspired us to search for an alternative method to identify MIPS: (1) computing the probability distribution function of particle displacement and (2) detecting the departures from Gaussianity, i.e., the two-dimensional non-Gaussian parameter α_2 [Eq. (7), expanding an idea we proposed in Ref. 51].

In Fig. 4(a), the probability distribution functions of particle displacements in the steady-state are shown for ABPs interacting via the WCA (left-hand side) and PHS (right-hand side) potentials at different values of Pe_{D_r} and density. When the system is in a homogeneous state ($\rho = 0.509$, $Pe_{D_r} = 20$, red), the PDF is clearly Gaussian, which is shown as a parabola in the semi-logarithmic plot. However, as soon as the system enters MIPS ($\rho = 0.64$, $Pe_{D_r} = 90$, blue, and $\rho = 1.02$, $Pe_{D_r} = 120$, black), the PDF has a non-Gaussian shape in which the contributions from the slow and fast-moving particles (those inside and outside the MIPS region, respectively) can be clearly detected.

In Figs. 4(b)–4(d), we show the time evolution of α_2 for ρ [from high (b) to low (d)] and Pe_{D_r} ranging from 10 (blue solid line) and 60 (red dashed line) to 120 (black dashed-dotted line). The measurements are taken starting from initial configurations in the steady-state for systems of particles interacting with the WCA (left-hand side) and PHS (right-hand side) potentials. In the insets, the thresholds of admissible non-Gaussianity are depicted as horizontal black lines, corresponding to ten times the size of fluctuations for a given system at the same density and in the absence of any activity. The choice of the factor of 10 is arbitrary but appears to be a reasonable choice if we assume that the distribution of instantaneous values of α_2 for a passive homogeneous system is Gaussian, and considering that, in a perfect Gaussian distribution, 99.7% of all α_2 values should be included within the $[-3\sigma_\alpha, 3\sigma_\alpha]$ interval. Excursions in the value of α_2 of sizes larger than $10\sigma_\alpha$ are thus indicative of non-Gaussianity in the particle displacements and, therefore, of dynamical heterogeneity and MIPS. Note that, although the systems

are in the steady-state, the instantaneous value of α_2 is not constant. Other equilibrium systems such as gels of associating polymers⁶¹ show a similar trend in which α_2 becomes greater than zero for a given time, before returning to zero at very long times.

For $Pe_{D_r} = 10$ (blue solid lines in Fig. 4), none of the three states for both WCA and PHS ends in a MIPS state (see Fig. 2), and the evolution of α_2 is within the threshold limits either at all times or after a short “equilibration” time equal to a few characteristic times between collisions. For $Pe_{D_r} = 60$ (red dashed lines in Fig. 4), none of the three states for the WCA potential is in a MIPS state (see Fig. 2) and α_2 is also within the threshold of non-Gaussianity. However, for the PHS potential, all three states present MIPS and α_2 shows clear signs of non-Gaussianity. At the density $\rho = 0.509$, the excursions of α_2 outside the limits are short-lived and reach moderate values, which is consistent with the fact that the point lies at the boundary of the MIPS region in the phase diagram of PHS (see Fig. 2). Finally, for $Pe_{D_r} = 120$ (black dashed-dotted lines in Fig. 4), all three states for both WCA and PHS show MIPS (see Fig. 2), and the evolution of α_2 is clearly non-Gaussian from very early times (as shown in Fig. 5 of the [supplementary material](#)).

Therefore, the results obtained with α_2 to establish whether the system is in a homogeneous state or MIPS state coincide with those obtained when computing the local density. The calculation of the non-Gaussian parameter is a straightforward method to identify MIPS states and computationally far less demanding than other methods such as computing probability distributions of local densities using Voronoi cells. In terms of computational requirements, both methods need the system to reach steady-state. On the one hand, in order to compute $P(\rho_0)$, one needs good statistics (long runs and uncorrelated configurations). On the other hand, α_2 is very easy to calculate (even included in LAMMPS⁵³), and MIPS can be detected without the need of very long runs and for a large number of particles. In MIPS states, α_2 rapidly becomes very large. In addition, we anticipate that the advantages of using the non-Gaussian parameter to detect MIPS over other static methods will be even clearer when simulating systems of ABP in three dimensions.

C. Dynamical features of MIPS

In Sec. III B, we show that when the system enters a MIPS phase, the non-Gaussian parameter is clearly non-zero, as expected for a system separating into a dilute region of fast particles and a dense region of slow particles. The appearance of dynamical heterogeneities is a characteristic feature of supercooled liquids approaching the glass transition.⁵⁶ Similarly, several studies have been performed on trying to understand the non-equilibrium glass transitions of active particles.^{72–78}

In Ref. 62, the authors studied the dynamics of a WCA-ABP binary mixture. They computed the effective diffusion coefficient as a function of packing fraction and found that, at low effective temperatures, the diffusion coefficient increased with the increase in persistence time (or activity). To determine the glass transition line, they fitted the diffusion coefficient to a Vogel–Fulcher-like dependence on the packing fraction, $\ln D = A + B(\phi - \phi_c)$, where A , B , and ϕ_c (the glass transition packing fraction) are the fitting parameters. From the data, the authors inferred that, at a low effective temperature, the glass transition packing fraction monotonically increased with activity.

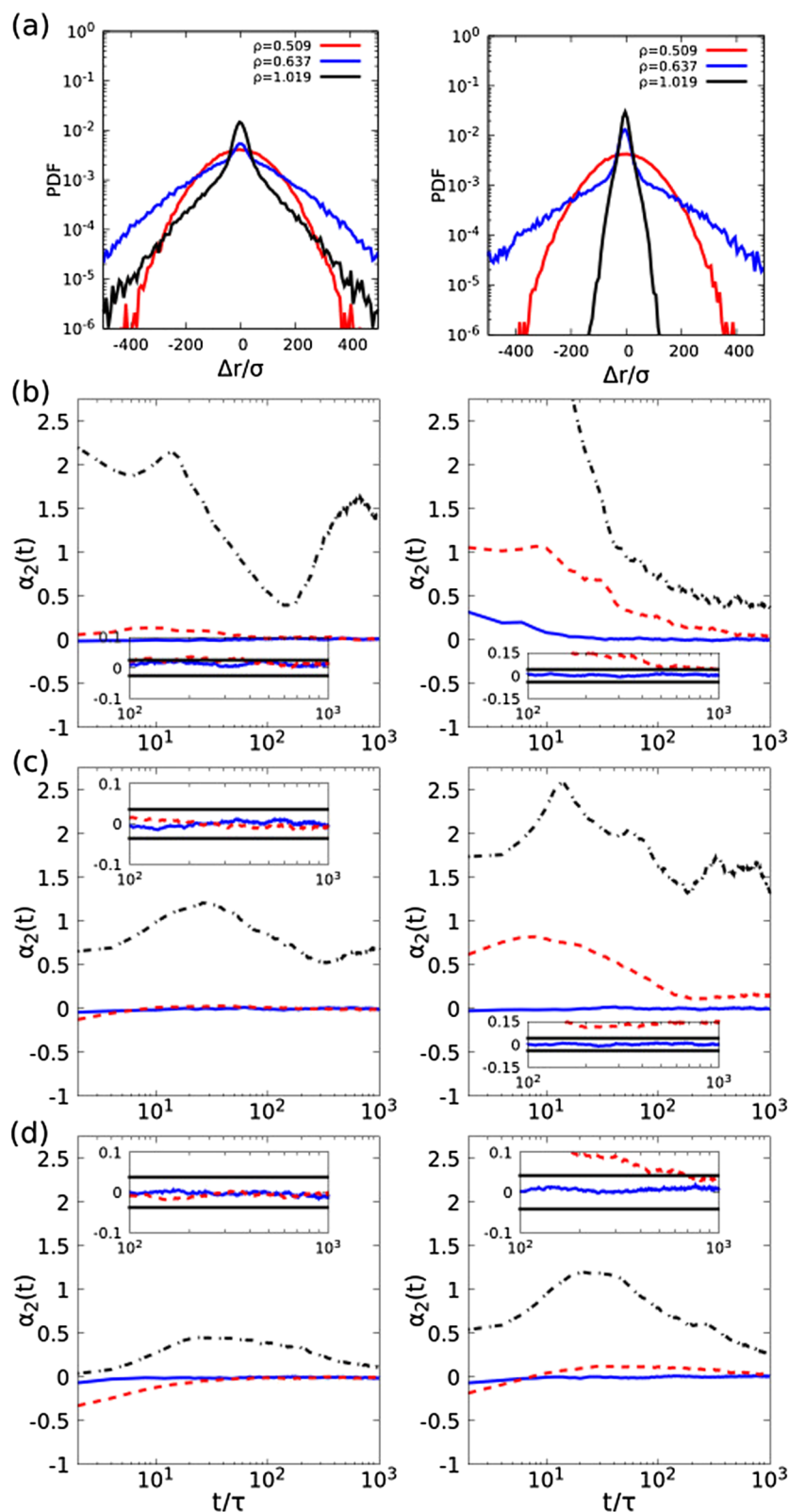


FIG. 4. (a) Steady-state probability distribution functions of particle displacements at different densities and Pe_{D_r} for WCA (left) and PHS (right): $\rho = 0.51$, $Pe_{D_r} = 20$ (red, homogeneous case), $\rho = 0.64$, $Pe_{D_r} = 90$ (blue, MIPS at a low packing fraction) and $\rho = 1.02$, $Pe_{D_r} = 120$ (black, MIPS at a high packing fraction) at the same lag time ($t = 128$). Time evolution of the 2D non-Gaussian parameter α_2 for systems of ABP interacting with the WCA (left) and the PHS (right) potentials at densities (b) $\rho = 1.019$, (c) $\rho = 0.764$, and (d) $\rho = 0.509$ and Pe_{D_r} values equal to 10 (blue solid line), 60 (red dashed line), and 120 (black dashed-dotted line). All simulations start in a stationary condition. The insets show a zoomed-in view of the last steps of the simulations (from $t = 100$ – 1000). Black horizontal lines show the threshold used to establish MIPS [$10\sigma_\alpha$, see the discussion after Eq. (7)].

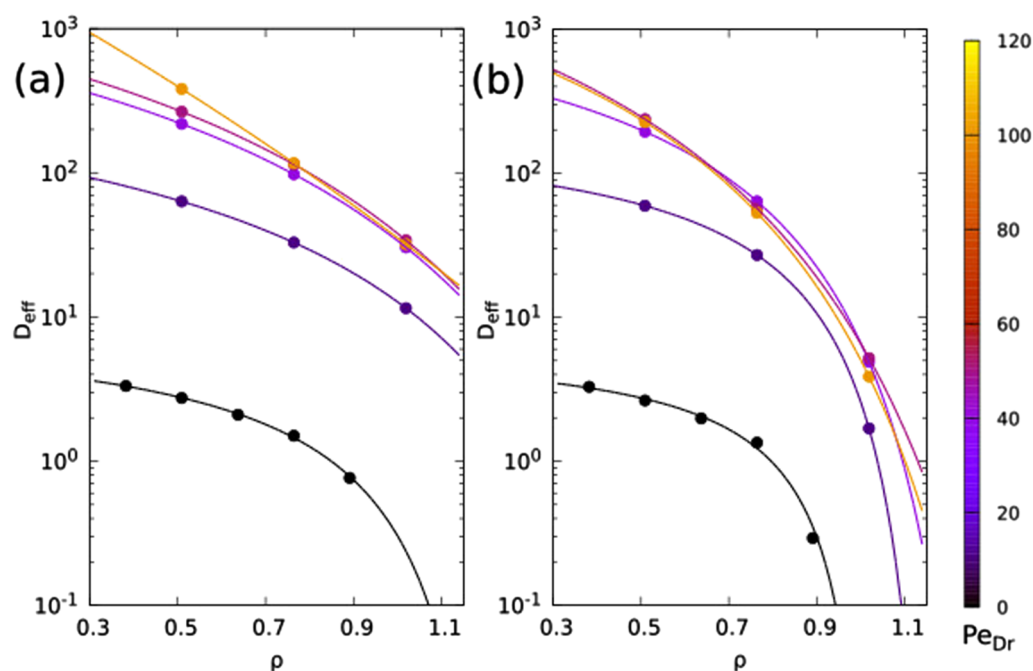


FIG. 5. Diffusion coefficient vs ρ for (a) WCA and for (b) PHS for $Pe_{Dr} = 0$ (black), 10 (dark-violet), 40 (light-violet), and 80 (orange). Lines are the Vogel–Fulcher model fit for these data. Note that this fit is performed with the results of simulations shown in Fig. 3.

As in Ref. 62, we study the dynamics by computing the mean-square displacement and extracting the effective diffusion coefficient from its long-time behavior. In Fig. 5, we represent the diffusion coefficient as a function of density for passive particles (black lines), particles in homogeneous states (purple lines), and particles in MIPS states (orange lines) when the Péclet number is varied by changing D_r .

When dealing with passive particles (black lines), unsurprisingly, the values of their diffusion coefficients are lower than those of active particles (colored lines). The diffusion coefficients of passive particles, when represented as a function of density, can be fitted by a Vogel–Fulcher expression.⁶² Interestingly, the stiffer potential (see the right panel in Fig. 5) reduces the effective diffusion at higher densities when aggregation becomes important. For the WCA potential (see the left panel in Fig. 5), the diffusion coefficient is significantly higher than for PHS at high densities, and this stems from the softer nature of the interaction, which allows a certain degree of particle overlap and an easier particle motion.

When dealing with active particles, effective diffusion is always higher for passive counterparts. Moreover, the effective diffusion for very low densities is identical in both potentials. At higher densities, a stiffer potential such as PHS is more efficient in preventing particle overlap and thus has a lower effective diffusion coefficient than a softer potential such as WCA. The Vogel–Fulcher equation seems to be a valid model to describe the decay of the effective diffusion coefficient with density (see the table in the supplementary material), even for active systems,⁶² except in the highest density/Péclet number regime. In this parameter range, the Vogel–Fulcher fit yields the equivalent of a glass transition density ρ_0 , which is too large

to have any physical meaning (see the table in the supplementary material), even considering the larger degree of overlap between WCA particles.

Therefore, we conclude that the PHS-ABP diffusion coefficient can be fitted by a Vogel–Fulcher expression in a more meaningful way than the WCA-ABP one (see table 2 of the supplementary material). Since this relationship is used to describe the behavior of fragile glasses, we suggest that, as in Ref. 79, a suspension of PHS-ABP behaves like a fragile glass, whereas this behavior is less clear when particles are softer (WCA-like).

It is important to note that the mean-square displacement in the presence of MIPS (orange lines in Fig. 5) is the result of the average between fast and slow phases. When dealing with passive systems close to the glass transition, the fraction of fast particles is extremely low. While the fast (dilute)/slow (dense) phases seem to be more equally present in WCA-ABP, in PHS-ABP, the MIPS state is characterized by small regions of low (fast) density immersed in a sea of high (slow) density. Therefore, the contribution of fast particles in the mean-square displacement is lower for PHS. For this reason, the VFT fits, which are supposed to work for passive colloidal glasses, are less meaningful for active colloids at high densities and activities, independent of the stiffness of the interaction potential.

IV. CONCLUSIONS

We have studied a two-dimensional suspension of repulsive ABPs interacting via two different repulsive potentials: WCA and a stiffer PHS potential. To characterize their structural features, we

have studied their phase behavior when varying the Péclet number in several ways.

We have found that, in addition to Pe and ρ , two other parameters have an effect on the onset of MIPS: the relative strength of the effective translational diffusion with respect to the self-propulsion force and the relative strength of the interaction forces with respect to the self-propulsion.

The translational diffusion hinders the emergence of MIPS, preventing its formation at low ρ and also shifting the MIPS boundary to higher Pe .

When the self-propulsion force is strong enough compared to the repulsive excluded volume interactions, the softness of the potential plays a role in the state diagram. When interacting via WCA, the overlapping of particles in the dense region induces a shift of the MIPS phase boundary to higher ρ . This effect can be avoided by choosing the stiffer PHS potential at the cost of having to use a smaller time step. Therefore, different repulsive potentials might lead to differences in the phase behavior and this is particularly the case when simulating “hard” active matter particles.

For increasing ρ , we identify the following states, independent of the interaction potential: dense phases of slow particles with low density clusters, bands, and bubbles of fast particles, in this order. For stiffer potentials such as PHS, these phenomena can be observed at lower densities. Note that the observed percolating bands always appear along the shortest dimension of the box, showing that this particular morphology could be the consequence a finite size effect.

To better characterize these morphologies, we compute the crystalline order, both local and global. The stiffness of the interaction potential not only has a considerable effect on the state diagram but also affects the particle order inside the dense phase. When comparing the two interaction potentials, WCA-ABP have a lower hexatic order than PHS ones at the same densities— Pe_{Dr} values. The reason is that WCA particles are allowed to partially overlap, different from PHS, which at a high density organize in a hexagonal order. In conclusion, ψ_6 cannot be used as a good indicator to locate the MIPS boundaries.

We suggest an alternative way to better identify the MIPS boundaries based on particle dynamics instead of local density. Since particle displacements should be Gaussian in homogeneous states, we inspect the value of the two-dimensional non-Gaussian parameter α_2 to detect MIPS. Our results show that both static and dynamic methods yield the same MIPS boundary. Using the non-Gaussian parameter is easier, less computationally expensive, and faster than other static methods, such as computing the local density.

Finally, we have studied the system dynamics and found that the effective diffusion coefficient can be fitted by a Vogel–Fulcher equation, as for over-compressed colloidal suspensions. However, this fit is less meaningful for active colloids at high densities and activities, independent of the stiffness of the interaction potential.

SUPPLEMENTARY MATERIAL

See the [supplementary material](#) for the clarification of the differences between the different ways of varying the Peclet number, clarification of the differences between the different ways of changing the Peclet number, with the state diagrams merged in the same

plot, and more details on both the structural and dynamical analysis performed to identify MIPS.

ACKNOWLEDGMENTS

The authors acknowledge funding from the MINECO and the UCM/Santander PR26/16-10B-2 under Grant Nos. FIS2016-78847-P and ID2019-105343GB-I00, respectively. F.A. acknowledges support from the “Juan de la Cierva” program (No. FJCI-2017-33580). R.M. acknowledges funding from the MICINN (Ministerio de Ciencia e Innovación, Spain, FPI Grant No. BES-2017-081108). The authors acknowledge the computer resources and technical assistance provided by the Centro de Supercomputación y Visualización de Madrid (CeSViMa) and the Red Española de Supercomputación (RES, Grant Nos. FI-2020-1-0015 and FI-2020-2-0032).

There are no conflicts to declare.

DATA AVAILABILITY

The data that support the findings of this study are available from the corresponding author upon reasonable request.

REFERENCES

- 1 S. Ramaswamy, *J. Stat. Mech.: Theory Exp.* **2017**, 054002.
- 2 C. Bechinger, R. Di Leonardo, H. Löwen, C. Reichhardt, G. Volpe, and G. Volpe, *Rev. Mod. Phys.* **88**, 045006 (2016).
- 3 T. Vicsek and A. Zafeiris, *Phys. Rep.* **517**, 71–140 (2012).
- 4 O. Dauchot and H. Löwen, *J. Chem. Phys.* **151**, 114901 (2019).
- 5 A. Snezhko and I. S. Aranson, *Nat. Mater.* **10**, 698–703 (2011).
- 6 G. Volpe, S. Gigan, and G. Volpe, *Am. J. Phys.* **82**, 659 (2014).
- 7 N. Narinder, J. R. Gomez-Solano, and C. Bechinger, *New J. Phys.* **21**, 093058 (2019).
- 8 N. Narinder, C. Bechinger, and J. R. Gomez-Solano, *Phys. Rev. Lett.* **121**, 078003 (2018).
- 9 H. C. Berg, *Random Walks in Biology* (Princeton University Press, 1993).
- 10 F. Ginot, A. Solon, Y. Kafri, C. Ybert, J. Tailleur, and C. Cottin-Bizonne, *New J. Phys.* **20**, 115001 (2018).
- 11 A. E. Patteson, A. Gopinath, M. Goulian, and P. E. Arratia, *Sci. Rep.* **5**, 15761 (2015).
- 12 J. L. Aragones, S. Yazdi, and A. Alexander-Katz, *Phys. Rev. Fluids* **3**, 083301 (2018).
- 13 P. Xu, S. Duan, Z. Xiao, Z. Yang, and W. Wang, *Soft Matter* **16**, 6082 (2020).
- 14 C. Calero, J. Garcia-Torres, A. Ortiz-Ambriz, F. Sagués, I. Pagonabarraga, and P. Tierno, *Soft Matter* **16**(16), 6673 (2020).
- 15 J. Palacci, C. Cottin-Bizonne, C. Ybert, and L. Bocquet, *Phys. Rev. Lett.* **105**, 088304 (2010).
- 16 F. Ginot, I. Theurkauff, D. Levis, C. Ybert, L. Bocquet, L. Berthier, and C. Cottin-bizonne, *Phys. Rev. X* **5**, 011004 (2015).
- 17 A. I. Campbell, S. J. Ebbens, P. Illien, and R. Golestanian, *Nat. Commun.* **10**, 3952 (2019).
- 18 A. R. Sprenger, M. A. Fernandez-Rodriguez, L. Alvarez, L. Isa, R. Wittkowski, and H. Löwen, *Langmuir* **36**, 7066 (2020).
- 19 J. Yan, M. Han, J. Zhang, C. Xu, E. Luijten, and S. Granick, *Nat. Mater.* **15**, 1095–1099 (2016).
- 20 M. N. van der Linden, L. C. Alexander, D. G. A. L. Aarts, and O. Dauchot, *Phys. Rev. Lett.* **123**, 098001 (2019).
- 21 H. R. Vutukuri, M. Lisicki, E. Lauga, and J. Vermant, *Nat. Commun.* **11**, 2628 (2020).
- 22 J. Palacci, S. Sacanna, S.-H. Kim, G.-R. Yi, D. J. Pine, and P. M. Chaikin, *Philos. Trans. R. Soc., A* **372**, 20130372 (2014).
- 23 M. E. Cates and J. Tailleur, *Europhys. Lett.* **101**, 20010 (2013).

- ²⁴A. Martín-Gómez, D. Levis, A. Díaz-Guilera, and I. Pagonabarraga, *Soft Matter* **14**, 2610 (2018).
- ²⁵P. Digregorio, D. Levis, A. Suma, L. F. Cugliandolo, G. Gonnella, and I. Pagonabarraga, *Phys. Rev. Lett.* **121**, 098003 (2018).
- ²⁶C. B. Caporusso, P. Digregorio, D. Levis, L. F. Cugliandolo, and G. Gonnella, *Phys. Rev. Lett.* **125**, 178004 (2020).
- ²⁷Y. Fily and M. C. Marchetti, *Phys. Rev. Lett.* **108**, 235702 (2012).
- ²⁸G. S. Redner, M. F. Hagan, and A. Baskaran, *Phys. Rev. Lett.* **110**, 055701 (2013).
- ²⁹J. Stenhammar, D. Marenduzzo, R. J. Allen, and M. E. Cates, *Soft Matter* **10**, 1489–1499 (2014).
- ³⁰J. Bialké, H. Löwen, and T. Speck, *Europhys. Lett.* **103**, 30008 (2013).
- ³¹J. T. Siebert, F. Dittrich, F. Schmid, K. Binder, T. Speck, and P. Virnau, *Phys. Rev. E* **98**, 030601 (2018).
- ³²A. Wysocki, R. G. Winkler, and G. Gompper, *Europhys. Lett.* **105**, 48004 (2014).
- ³³N. de Macedo Biniossek, H. Löwen, T. Voigtman, and F. Smallenburg, *J. Phys.: Condens. Matter* **30**, 074001 (2018).
- ³⁴D. Levis, J. Codina, and I. Pagonabarraga, *Soft Matter* **13**, 8113–8119 (2017).
- ³⁵P. Digregorio, D. Levis, A. Suma, L. F. Cugliandolo, G. Gonnella, and I. Pagonabarraga, *J. Phys.: Conf. Ser.* **1163**, 012073 (2019).
- ³⁶S. Auer and D. Frenkel, *J. Phys.: Condens. Matter* **14**, 7667 (2002).
- ³⁷A.-P. Hynninen and M. Dijkstra, *Phys. Rev. E* **68**, 021407 (2003).
- ³⁸S. Prestipino, F. Saija, and P. V. Giaquinta, *J. Chem. Phys.* **123**, 144110 (2005).
- ³⁹J. Taffs, S. R. Williams, H. Tanaka, and C. P. Royall, *Soft Matter* **9**, 297–305 (2013).
- ⁴⁰H. C. Andersen, J. D. Weeks, and D. Chandler, *Phys. Rev. A* **4**, 1597–1607 (1971).
- ⁴¹P. N. Pusey and W. van Megen, *Nature* **320**, 340–342 (1986).
- ⁴²J. Bialké, T. Speck, and H. Löwen, *Phys. Rev. Lett.* **108**, 168301 (2012).
- ⁴³L. Filion, M. Hermes, R. Ni, and M. Dijkstra, *J. Chem. Phys.* **133**, 244115 (2010).
- ⁴⁴S. Pieprzyk, M. N. Bannerman, A. C. Brańka, M. Chudak, and D. M. Heyes, *Phys. Chem. Chem. Phys.* **21**, 6886–6899 (2019).
- ⁴⁵L. Filion, R. Ni, D. Frenkel, and M. Dijkstra, *J. Chem. Phys.* **134**, 134901 (2011).
- ⁴⁶J. D. Weeks, D. Chandler, and H. C. Andersen, *J. Chem. Phys.* **54**, 5237–5247 (1971).
- ⁴⁷J. Jover, A. J. Haslam, A. Galindo, G. Jackson, and E. A. Müller, *J. Chem. Phys.* **137**, 144505 (2012).
- ⁴⁸J. R. Espinosa, C. Vega, C. Valeriani, and E. Sanz, *J. Chem. Phys.* **144**, 034501 (2016).
- ⁴⁹P. Rosales-Pelaez, P. M. de Higes, E. Sanz, and C. Valeriani, *J. Stat. Mech.: Theory Exp.* **2016**, 094005.
- ⁵⁰P. M. de Higes, P. Rosales-Pelaez, C. Valeriani, P. N. Pusey, and E. Sanz, *Phys. Rev. E* **96**, 020602 (2017).
- ⁵¹D. Rogel Rodríguez, F. Alarcon, R. Martinez, J. Ramirez, and C. Valeriani, *Soft Matter* **16**, 1162–1169 (2020).
- ⁵²J. A. Barker and D. Henderson, *J. Chem. Phys.* **47**, 2856 (1967).
- ⁵³S. Plimpton, *J. Comput. Phys.* **117**, 1 (1995).
- ⁵⁴H. Brenner, *J. Colloid Sci.* **20**, 104–122 (1965).
- ⁵⁵F. Ginelli and H. Chaté, *Phys. Rev. Lett.* **105**, 168103 (2010).
- ⁵⁶L. Berthier and G. Biroli, *Rev. Mod. Phys.* **83**, 587 (2011).
- ⁵⁷S. K. Kumar, G. Szamel, and J. F. Douglas, *J. Chem. Phys.* **124**, 214501 (2006).
- ⁵⁸S. Song, S. J. Park, M. Kim, J. S. Kim, B. J. Sung, S. Lee, J.-H. Kim, and J. Sung, *Proc. Natl. Acad. Sci. U. S. A.* **116**, 12733–12742 (2019).
- ⁵⁹B. Vorselaars, A. V. Lyulin, K. Karatasos, and M. A. J. Michels, *Phys. Rev. E* **75**, 011504 (2007).
- ⁶⁰E. R. Weeks, J. C. Crocker, A. C. Levitt, A. Schofield, and D. A. Weitz, *Science* **287**, 627–631 (2000).
- ⁶¹J. Ramirez, T. J. Dursch, and B. D. Olsen, *Macromolecules* **51**, 2517–2525 (2018).
- ⁶²L. Berthier, E. Flenner, and G. Szamel, *New J. Phys.* **19**, 125006 (2017).
- ⁶³S. A. Morley, D. A. Venero, J. M. Porro, S. T. Riley, A. Stein, P. Steadman, R. L. Stamps, S. Langridge, and C. H. Marrows, *Phys. Rev. B* **95**, 104422 (2017).
- ⁶⁴V. Prymidis, H. Sielcken, and L. Filion, *Soft Matter* **11**, 4158 (2015).
- ⁶⁵At very high densities, PHS particles barely move. Therefore, one should make sure to prepare an initial configuration where almost no crystalline particles are present. At such high densities, one should resort to special numerical techniques (such as the one by Ref. 80) to prepare an initial configuration in an amorphous phase. Eventually, the amorphous solid might crystallize. As with PHS, a crystalline phase might also be detected for WCA at densities even closer to the closed packed state (since particles are allowed to partially overlap). However, studying the crystallization of a monodisperse suspension of active repulsive spheres was not the goal of our study, and for this reason, we have not characterized the state of the system at such high densities.
- ⁶⁶A. Rahman, *Phys. Rev.* **136**, A405 (1964).
- ⁶⁷C. Donati *et al.*, *Phys. Rev. Lett.* **80**, 2338 (1998).
- ⁶⁸C. Donati, S. C. Glotzer, and P. H. Poole, *Phys. Rev. Lett.* **82**, 5064 (1999).
- ⁶⁹A. H. Marcus, J. Schofield, and S. A. Rice, *Phys. Rev. E* **60**, 5725 (1999).
- ⁷⁰W. K. Kegel and A. van Blaaderen, *Science* **287**, 290 (2000).
- ⁷¹S. Henkes, Y. Fily, and M. C. Marchetti, *Phys. Rev. E* **84**, 040301 (2011).
- ⁷²T. E. Angelini, E. Hannezo, X. Treppe, M. Marquez, J. J. Fredberg, and D. A. Weitz, *Proc. Natl. Acad. Sci. U. S. A.* **108**, 4714 (2011).
- ⁷³R. Ni, M. A. C. Stuart, and M. Dijkstra, *Nat. Commun.* **4**, 2704 (2013).
- ⁷⁴Y. Fily, S. Henkes, and M. C. Marchetti, *Soft Matter* **10**, 2132 (2014).
- ⁷⁵E. Flenner, G. Szamel, and L. Berthier, *Soft Matter* **12**, 7136 (2016).
- ⁷⁶D. Bi, X. Yang, M. C. Marchetti, and M. L. Manning, *Phys. Rev. X* **6**, 021011 (2016).
- ⁷⁷R. Mandal, P. J. Bhuyan, P. Chaudhuri, M. Rao, and C. Dasgupta, *Phys. Rev. E* **96**, 042605 (2017).
- ⁷⁸H. Ding, H. Jiang, and Z. Hou, *Phys. Rev. E* **95**, 052608 (2017).
- ⁷⁹J. Mattsson, H. M. Wyss, A. Fernandez-Nieves, K. Miyazaki, Z. Hu, D. R. Reichman, and D. A. Weitz, *Nature* **462**, 83 (2009).
- ⁸⁰B. D. Lubachevsky and F. H. Stillinger, *J. Stat. Phys.* **60**, 561–583 (1990).